nature ecology & evolution

Article

https://doi.org/10.1038/s41559-025-02676-w

Simulated early Earth geochemistry fuels a hydrogen-dependent primordial metabolism

Received: 6 November 2024

Accepted: 7 March 2025

Published online: 30 April 2025

Check for updates

Vanessa Helmbrecht[1], Robert Reichelt[2], Dina Grohmann[2] & William D. Orsi[1,3]

Molecular hydrogen is the electron donor for the ancient exergonic reductive acetyl-coenzyme A pathway (acetyl-CoA pathway), which is used by hydrogenotrophic methanogenic archaea. How the presence of iron-sulfides influenced the acetyl-CoA pathway under primordial early Earth geochemistry is still poorly understood. Here we show that the iron-sulfides mackinawite (FeS) and greigite (Fe_3S_4), which formed in chemical garden experiments simulating geochemical conditions of the early Archaean eon (4.0–3.6 billion years ago), produce abiotic H_2 in sufficient quantities to support hydrogenotrophic growth of the hyperthermophilic methanogen *Methanocaldococcus jannaschii*. Abiotic H_2 from iron-sulfide formation promoted CO_2 fixation and methanogenesis and induced overexpression of genes encoding the acetyl-CoA pathway. We demonstrate that H_2 from iron-sulfide precipitation under simulated early Earth hydrothermal geochemistry fuels a H_2-dependent primordial metabolism.

Formation of iron-sulfide minerals is an ancient and globally widespread process known to proceed via mackinawite (FeS)[1] and the intermediate greigite (Fe_3S_4) (refs. 2,3) while producing H_2 (refs. 4–7). The ancient occurrence of hydrothermal iron-sulfide rich deposits in the geological record extend into the early Archaean Eon (Eoarchaean 4.0–3.6 billion years ago) and exhibit fossil features interpreted as some of the oldest signatures for life on Earth[8,9]. Chemical garden experiments have shown the mackinawite–greigite transition under hydrothermal conditions analogous to Eoarchaean geochemical environments[7,10]. Such iron-sulfide chemical gardens are mixtures of inorganic chemicals which often form precipitates resembling organic structures and have been applied in emergence of life studies to better understand connections between aqueous geochemistry and mineralogy in simulated hydrothermal springs[10,11]. However, links between abiotic H_2 production in iron-sulfide chemical gardens simulating Eoarchaean hydrothermal systems and early life are scarce.

Molecular H_2 can be produced abiotically in numerous geological environments, most notably by serpentinization involving mafic (Mg and Fe-rich) or ultramafic rocks[12,13]. Since their discovery in 1977[14], seafloor hydrothermal springs venting abiotic H_2 were viewed as potential energy sources and setting for the emergence of life[15–19]. Reactive iron-sulfide minerals are ubiquitous in hydrothermal vent black-smoker chimneys, which are surrounded by metalliferous sediments underlying the hydrothermal plumes of precipitated black iron-sulfide particles[15,20,21]. Modern black smokers can exhibit natural variations in fluid chemistry and temperature within a single vent system[22], providing temperature gradients and sources of chemical energy[15,16,21] to support a high diversity of microorganisms, including methanogenic archaea[20]. The availability of H_2 plays a key role as the main source of electrons for biological systems and thereby microbial growth at hydrothermal systems[23,24].

Models of early metabolism in the Eoarchaean predict that abiotic H_2 was a potentially important electron donor and CO_2 served as a key electron acceptor for the first cells[25–27]. Anaerobic organisms that use the H_2-dependent reductive acetyl-coenzyme A (acetyl-CoA) pathway for CO_2 fixation, such as methanogens and acetogens, are modern representatives that have preserved vestiges of the first metabolisms[28,29]. Geochemical evidence has shown that methanogenic microbes have

[1]Department of Earth and Environmental Sciences, Ludwig-Maximilians-Universität München, Munich, Germany. [2]Institute of Biochemistry, Genetics and Microbiology, Institute of Microbiology and Archaea Centre, Single-Molecule Biochemistry Lab and Regensburg Center for Biochemistry, University of Regensburg, Regensburg, Germany. [3]GeoBio-CenterLMU, Ludwig-Maximilians-Universität München, Munich, Germany. e-mail: w.orsi@lrz.uni-muenchen.de

been present since the early Archaean at least 3.5 billion years ago[29], and it has been proposed that methanogens could have emerged in an iron-sulfide hydrothermal black-smoker environment[16]. Furthermore, physiological predictions of the last universal common ancestor (LUCA) based on genome data indicated that LUCA was possibly (hyper) thermophilic[30], anaerobic and H_2-dependent[31], and used the acetyl-CoA pathway to fix CO_2 (refs. 27,31–34). The acetyl-CoA pathway is the most ancient among carbon-fixation pathways[35], as it is short, non-cyclic, exergonic[33,35,36] and the only carbon-fixation pathway that can be reconstituted in the laboratory to take place without enzymes[25,37].

The acetyl-CoA pathway is furthermore replete with enzymes that depend on simple Fe(Ni)S cofactors[27,31,33,36,38]. For example, the CO_2 reducing-and-fixing enzyme formylmethanofuran dehydrogenase in methanogens contains an anomalously high 46 [4Fe–4S] clusters[39]. Other enzymes such as ferredoxin and CO dehydrogenase, which are common to methanogens, have iron-sulfur clusters with similar structure to iron-sulfide minerals, such as mackinawite and greigite[18,36], which form in hydrothermal environments. These observations have led to the hypothesis that iron-sulfide clusters in these modern enzymes might be relics of an ancient metabolism, which possibly originated in an ancient iron-sulfide rich setting[31,40].

These data and observations suggest an ancient origin of the acetyl-CoA pathway as a potential primordial metabolism[25,32–35,41]. Because of the possibility that hyperthermophilic methanogens harbour one of the most ancient metabolisms[30], we investigated acetyl-CoA pathway-dependent growth of the methanogenic hyperthermophile *Methanocaldococcus jannaschii* during iron-sulfide mineral formation.

Ferruginous (anoxic and iron-rich[42]) Archaean oceans contained dissolved ferrous iron concentrations of 0.1–10 mM (refs. 43,44). Sulfide may have been relatively rare as shown by its apparent dearth in the Hadean and Eoarchaean, but the origin of sulfide could have been derived from volcanic sulfur dioxide and polymerized sulfides[45,46]. In the absence of sulfidic fluids, green rust was probably a major constituent of Hadean and Archaean chemical gardens under ferruginous conditions[47,48]. Sulfate was extremely rare in the Archaean oceans[49], and the salinity has been predicted to be similar[50] if not greater[51] than now found in ocean water. We attempted to reflect these ancient conditions of the Eoarchaean oceans in our chemical gardens (Supplementary Methods).

As our model organism, we chose the methanogenic hyperthermophile *M. jannaschii* (DSM strain 2661), which was originally isolated from hydrothermal iron-sulfide sediment at the base of a black smoker on the East Pacific Rise[52]. *M. jannaschii* serves as a model organism for methanogenesis[53–55]; it uses H_2 and CO_2 as its sole carbon and energy source and has an optimal growth temperature ~85 °C (refs. 52). Thus, tracing both H_2 and CO_2 and the product CH_4 can reveal the active metabolism of this organism in controlled experiments, which is advantageous, because only a small amount of substrates and products need to be measured to study the energy metabolism.

Results and discussion

Iron-sulfide chimney formation, mineralogy and habitability

To precipitate iron-sulfide, we created sulfidic precipitation mounds (experiment 1, Supplementary Table 1) within a ferruginous aqueous environment germane to hydrochemical conditions predicted for the Hadean Ocean at the time of the origin of life[7,10,18]. Acidic sulfidic solution (0.5 M Na_2S, pH 3) was injected into an amorphous ferruginous solution (0.5 M $Fe(II)Cl_2$, pH 6) (chimney protocol in Supplementary Methods). Within 10 min, iron-sulfide minerals crystallized forming a black-chimney structure reaching an average height of 2.0 cm (s.d. = 0.1). In this initial phase of the experiment, the chimney showed the most rapid growth (growth rate = 0.2 cm min^{-1}). After 1 hour, the average height of the chimney was 2.5 cm (s.d. = 0.1, growth rate = 0.01 cm min^{-1}). No growth of the chimney was observed after 1 hour. All experiments were performed under an anoxic N_2 atmosphere in an anoxic chamber. Additional information about imaging, processing and quantifying the chimney growth is displayed in the Supplementary Methods.

The chimneys were stable at room temperature. Upon heating of the injection fluid, however, bubbles formed in the sulfidic fluid and caused the chimney structures to collapse into sediment, which collected at the bottom of the flask. Therefore, all hydrothermal experiments at 80 °C were conducted using sedimented iron-sulfide material (for details of preparation, see experiments 2, 3, 4 and 5 in Supplementary Table 1), which we describe as 'sedimentary iron-sulfide chemical gardens'. Future experiments could test if higher pressure (similar to the deep sea) would increase the boiling temperature of the injected sulfidic fluid and reduce formation of gas bubbles.

Raman spectroscopy and scanning electron microscopy (SEM) revealed that the hydrothermal (80 °C) sedimentary iron-sulfide chemical gardens (experiment 5a, Supplementary Table 1) comprised mostly mackinawite (FeS) and greigite (Fe_3S_4), with traces of NaCl (Fig. 1c–f). Under anoxic conditions, metastable mackinawite, an iron-monosulfide precursor, transforms into greigite when heated to 70–75 °C through partial oxidation of mackinawite with water[2,7].

Mackinawite is a tetragonal iron-monosulfide[1]. Greigite is the cubic thio-spinel of iron, exhibiting mostly octahedral and sometimes cubic crystals[2,3,56]. Next to the Raman peaks for mackinawite at 212, 275–276, 385–386 and 583–584 cm^{-1} (Fig. 1c)[57,58] a broad peak at 1,300 cm^{-1} was evident of slight laser beam oxidation of the sample, which converted mackinawite into haematite (Fe_2O_3). The greigite Raman spectra (Fig. 1d) show peaks at 191, 250, 299–301 and 350–354 cm^{-1} (refs. 7,59). The Raman images display an octahedral crystal morphology fitting for greigite[3] (Fig. 1e). The energy dispersive X-ray (EDX) spectrum highlights the presence of iron (30.78 at.%) and sulfur (41.33 at.%) in the sample (Fig. 1f). Magnetic properties of the iron-sulfide minerals from the chemical garden (experiment 5a, Supplementary Table 1) was confirmed with a 96-ring magnet plate (ALPAQUA) (Extended Data Fig. 1), indicating the presence of greigite, which is a ferrimagnetic mineral[2,56,60,61]. These results are consistent with earlier chemical garden experiments[7], which also produced semipermeable colloidal membranes of iron-monosulfide minerals mimicking natural hydrothermal chimneys[10].

Iron-sulfur clusters play a critical role in various metalloenzymes that are present in both archaea and bacteria[7], and therefore mackinawite and greigite are considered key minerals for the emergence of life[7,40,59,62] because they structurally resemble active centres of proteins and enzymes[36,59,63,64]. The presence of both minerals in hydrothermal environments hints at the possibility that iron-rich cofactors in proteins and enzymes geologically originate from mineral precursors[63]. It is therefore notable that mackinawite and greigite are the major precipitated minerals in our chemical gardens simulating sulfidic Eoarchaean hydrothermal springs (Fig. 1d). We note that the pyrite structure is different because the ferrous iron is ligated to six sulfur pairs, which makes the mineral less reactive by comparison[65].

To test the habitability of the sedimentary iron-sulfide chemical gardens, we added stationary-phase culture of the hyperthermophilic methanogen *M. jannaschii*[52] to the chemical gardens (experiment 4a, Supplementary Table 1). Fluorescence microscopy revealed *M. jannaschii* cells physically associated with iron-sulfide particles (Fig. 1b), consistent with minerals found in black smokers that are colonized by thermophilic archaea[66,67]. The pH of the sedimentary chemical gardens was 5.5, which is close to the optimal pH for growth of *M. jannaschii*[68]. Next, we investigated mechanisms linking the mineralogy of the iron-sulfide chemical gardens to microbial habitability.

Abiotic H_2 production and methanogenesis in chemical gardens

We detected hydrogen gas (H_2) emanating from the sedimentary iron-sulfide chemical gardens (experiment 2, Supplementary Table 1) in

https://doi.org/10.1038/s41559-025-02676-w

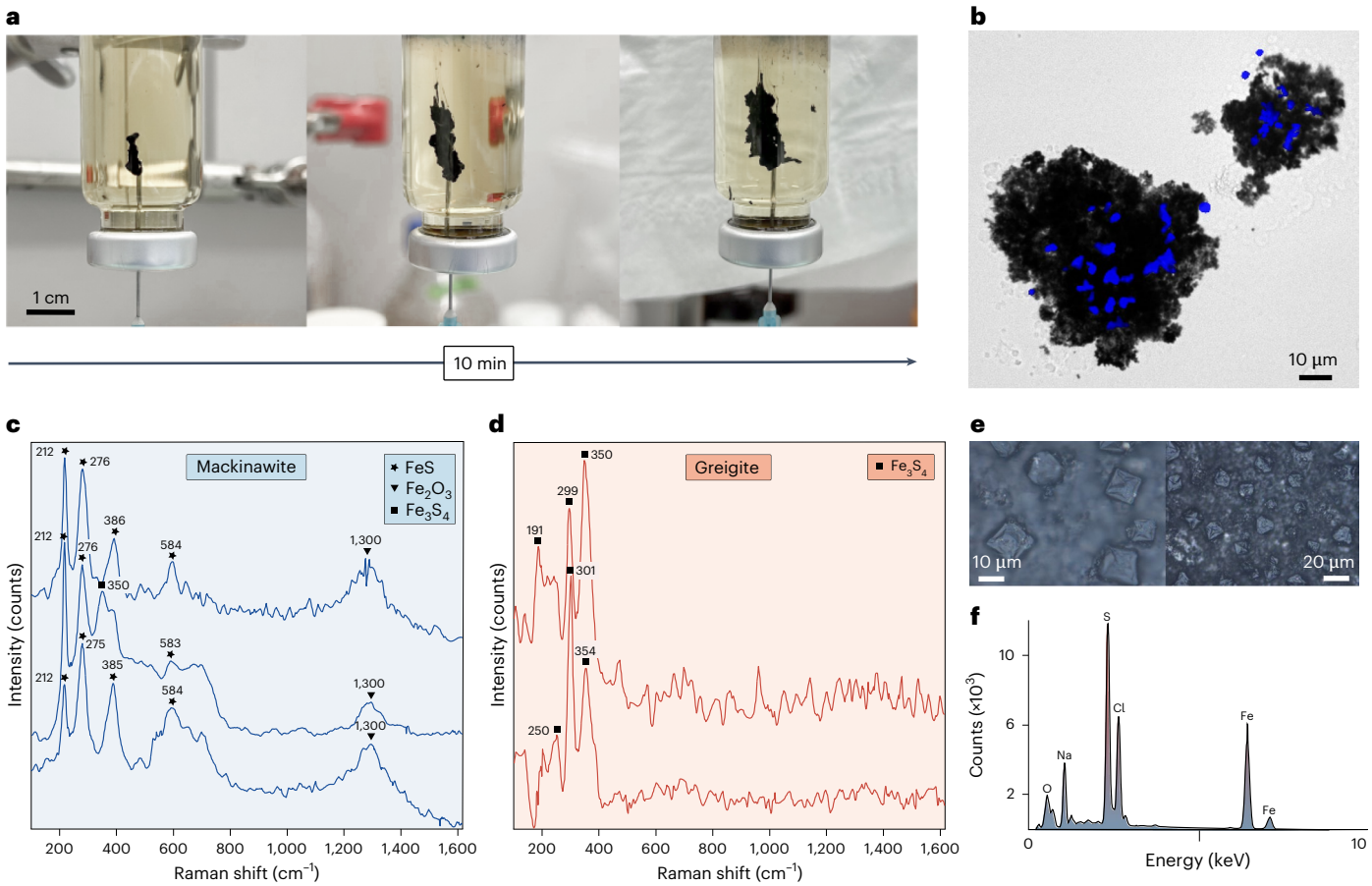

Fig. 1 | Iron-sulfide chimney formation, mineralogy and microbial colonization. **a**, Iron-sulfide chimney precipitated over the course of 10 min at 25 °C (experiment 1, Supplementary Table 1). The three images (from left to right) were taken 1, 5 and 10 min after the injection started. After 10 min, the chimney reached a height of 2.0 cm (s.d. = 0.1). **b**, *M. jannaschii* cells accumulate on iron-sulfide particles (experiment 4a). Overlay of a bright field image of the iron-sulfide particles and a fluorescence image of the cells. This was observed across three experimental replicates (Methods). **c**–**f**, Mineralogical analysis (experiment 5a). **c**,**d**, Raman spectroscopy identifies that mackinawite (FeS, **c**) and greigite (Fe_3S_4, **d**) are the primary minerals formed in the sedimentary iron-sulfide chemical gardens at 80 °C. This was observed across three experimental replicates (Supplementary Table 1). Important Raman peaks are labelled for mackinawite and greigite[7,57–59]. The peak at 1,300 cm^{-1} is due to laser beam oxidation. **e**, Raman images of a sedimentary iron-sulfide chemical garden. Most crystals have an octahedral shape typical for greigite. **f**, EDX of iron-sulfide particles with peaks indicating relative abundances of O, Na, S, Cl and Fe. keV, kiloelectron volt.

amounts proportional to the concentrations of Fe(II) and Na_2S (Fig. 2a). Abiotic H_2 was only detectable in flasks where no headspace was present (Supplementary Methods), which could be due to increasing pressure building without a larger headspace volume. The concentration of abiotic H_2 produced in the chemical gardens ranged from 124 ± 1 to 781 ± 138 µM, spanning Fe(II) and Na_2S concentrations of 10–500 mM, respectively ($P = 0.0206$) (Fig. 2a). This is in the range of H_2 concentrations in the fluids of black smokers, from 0.05 to 1 mM (ref. 12). Abiotic H_2 production is probably explained by the presence of mackinawite (FeS) and greigite (Fe_3S_4) above 70 °C (Fig. 1c,d), namely that H_2 is released during the hydration of iron-monosulfide[6,7,69] according to:

$$4FeS + 2H_2O \rightarrow Fe_3S_4 + Fe(OH)_2 + H_2$$

A similar reaction of mackinawite and H_2S was found to be used in an anaerobic metabolism by H_2-producing bacteria in a syntrophic partnership with hydrogenotrophic methanogens[70]. Addition of stationary-phase *M. jannaschii* culture to the chemical garden reduced abiotic H_2 significantly compared to controls ($P = 0.0001$) without added methanogens (Extended Data Fig. 2), indicating that the hydrogenotrophic *M. jannaschii* cells consume H_2 for growth. Others[54] defined the lower limit for growth at 17–23 µM of H_2, which is less H_2 than the iron-sulfide chemical gardens produced (experiment 2, Fig. 2a). No H_2 was detectable in controls where $FeCl_2$ and Na_2S were not added. We investigated the effects of abiotic H_2 from the sedimentary chemical gardens on the physiology of *M. jannaschii* (experiment 3, Fig. 2c) by tracking the production of H_2 and $^{13}CH_4$ at 80 °C (experiment 3, Supplementary Table 1) using $^{13}CO_2$ carbon substrate. After inoculation, an increase in $^{13}CH_4$ was observed concomitant with a decrease in $^{13}CO_2$, as expected for *M. jannaschii* methanogenesis (Fig. 2c). Over the course of 10 h, ^{13}C-labelled CO_2 decreased constantly, while abiotic H_2 increased in concentration until 4 h, after which the rate of H_2 consumption by *M. jannaschii* began to outpace H_2 production. We observed a direct correlation ($R^2 = 0.97$, $P < 0.005$) between abiotic H_2 produced by the chemical garden and ^{13}C-labelled CH_4 produced by *M. jannaschii* (Fig. 2b) indicating that, consistent with earlier studies[54,55], hydrogenotrophic methanogenesis by *M. jannaschii* in the iron-sulfide chemical gardens was limited by H_2.

M. jannaschii growth in iron-sulfide chemical gardens

We compared the growth of *M. jannaschii* at 80 °C in the iron-sulfide chemical garden (experiment 5a) to growth in MMC medium (experiment 5c) as a positive control and sterile water (experiment 5b) as a negative control. Similar to experiment 4, the sterile water negative control was used to account for the dilution factor introduced by inoculating the stationary-phase culture into the chemical garden, making

https://doi.org/10.1038/s41559-025-02676-w

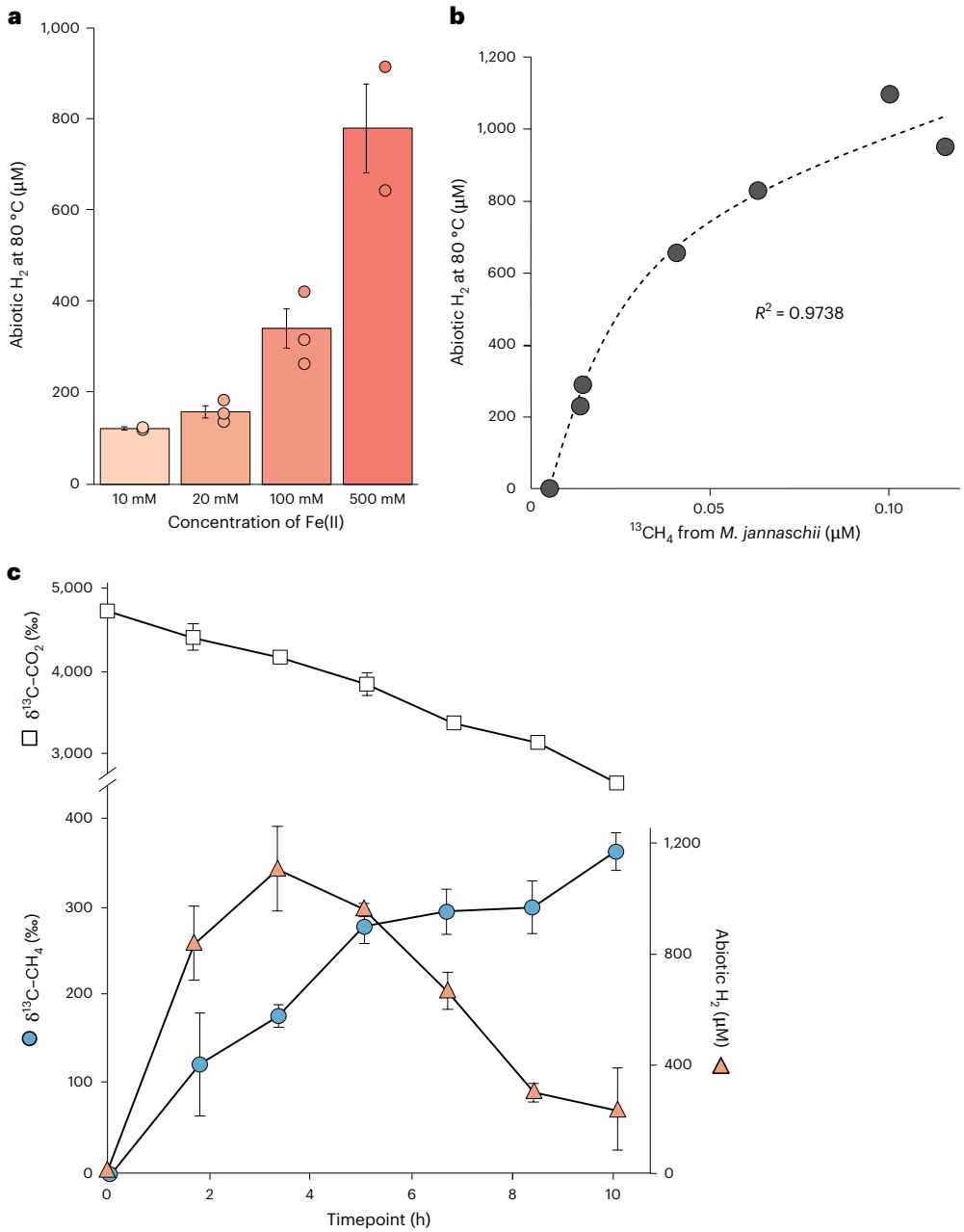

Fig. 2 | Abiotic H_2 produced by the iron-sulfide chemical garden fuels CO_2 reduction and methanogenesis by *M. jannaschii*. **a**, Production of abiotic H_2 in the chemical gardens increases with increasing Fe(II) concentrations at 80 °C (experiment 2, Supplementary Table 1). Error bars indicate standard error of the means, individual points represent biological replicates ($n = 3$). **b**, The concentration of abiotic H_2 produced in the sedimentary iron-sulfide chemical garden (500 mM $FeCl_2$ and Na_2S, 80 °C) correlates positively with the amount of $^{13}CH_4$ produced by *M. jannaschii*. **c**, Gas consumption and production by *M. jannaschii* in the sedimentary iron-sulfide chemical gardens at 80 °C supplemented with ^{13}C-bicarbonate to trace CO_2 fixation and methanogenesis (experiment 3). Error bars represent standard deviations across three biological replicates. Note that the ^{13}C-labelling of CO_2 decreases over time, as the ^{13}C-labelling of methane increases, indicating a transfer of ^{13}C from CO_2 to CH_4 by *M. jannaschii*. The abiotically produced H_2 increases over the first 4 h and then decreases afterwards, due to consumption by *M. jannaschii*.

the presence of iron-sulfide the only difference between experiments 5a and 5b (Supplementary Table 1).

M. jannaschii reached exponential growth (growth rate $\mu = 0.14\ h^{-1}$) in the iron-sulfide chemical gardens after 24 h reaching a peak cell concentration of 2.3×10^7 cells ml^{-1} (Fig. 3a) (experiment 4a, Supplementary Table 1). However, the growth rate in the chemical gardens (experiment 4a) was 30% lower ($P = 0.0424$) than the positive controls ($\mu = 0.20\ h^{-1}$), where *M. jannaschii* was grown in their standard MMC growth medium (experiment 4c) and reached a peak cell concentration of 3.0×10^7 cells ml^{-1}, lower than previous reports[52] possibly because we did not shake cultures during incubation. The lower growth rate in the iron-sulfide chemical gardens (Fig. 3a) could be explained by the lack of additional salts, trace metals (for example, Ni, Mo, Co, W and Zn) and nutrients compared to MMC medium, where nitrogen in the form of ammonia was present at tenfold higher concentrations[68]. Traces of nitrogen and other essential metals were inevitably transferred with the inoculum to the chemical gardens and were probably available—albeit at ultra-low concentrations—for growth (Fig. 3a).

No growth was observed in the negative (water) control (experiment 4b) (Fig. 3a). Because the addition of $Fe(II)Cl_2$ and Na_2S are the only

https://doi.org/10.1038/s41559-025-02676-w

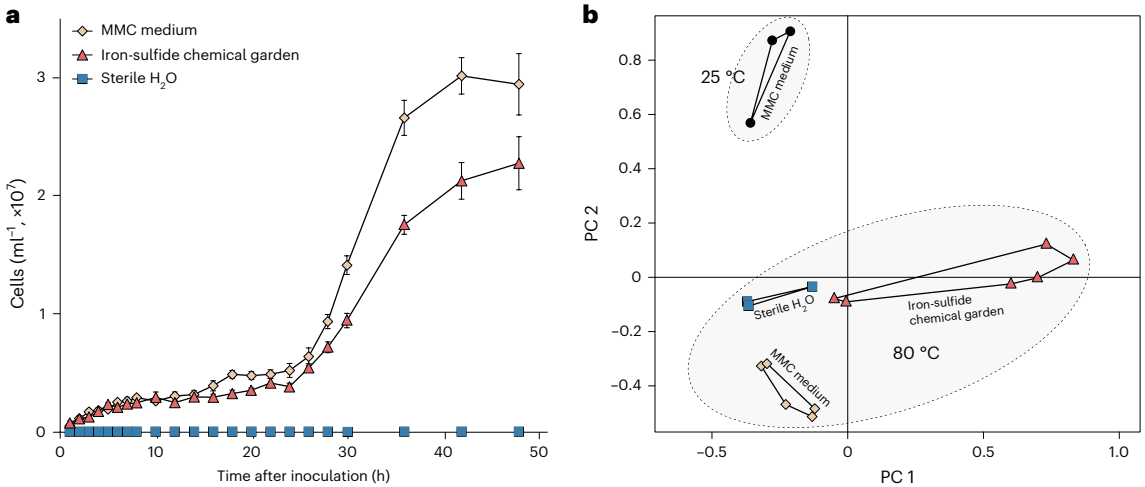

Fig. 3 | *M. jannaschii* growth and gene expression in the sedimentary iron-sulfide chemical gardens compared to controls. a, Comparison of *M. jannaschii* growth in three experimental settings: sedimentary iron-sulfide chemical gardens (experiment 4a, Supplementary Table 1), MMC growth medium (experiment 4c) and sterile water (experiment 4b). All experiments were performed at 80 °C, error bars indicate standard error of the means across three biological replicates. **b**, Principal-component (PC) analysis shows the significant difference of *M. jannaschii* gene expression in non-identical treatments (experiment 5) (analysis of similarity $P = 0.001$). Grey circles highlight transcriptomes from 25 and 80 °C experiments, respectively. Coloured symbols correspond to the same three experimental conditions that are displayed in **a** (yellow diamonds, MMC media control; orange triangles, iron-sulfide chemical garden; blue squares, sterile water negative control).

parameters that differed compared to the control (additional nutrients, vitamins or trace metals above those present in the inoculum were not added to the chemical gardens), exponential growth in the chemical gardens can be attributed to H_2 from the reaction of $FeCl_2$ and Na_2S (Fig. 2c and Extended Data Fig. 2). Nitrogen limitation cannot explain the large difference in growth rate between the water control and the chemical garden, because both experiments received the same amount of inoculum. This indicates that the growth in the chemical gardens was mainly limited by H_2 compared to nitrogen, indicating that the abiotic H_2 from the chemical garden was sufficient enough to rescue *M. jannaschii* from H_2 limitation.

Gene expression in iron-sulfide chemical gardens

RNA was extracted from the 80 °C sterile water control (experiment 5b), 10 mM iron-sulfide chemical garden (experiment 5a) and MMC medium (experiment 5c), which was determined to be 2.52, 2.90 and 10.00 ng μl^{-1}, respectively (Supplementary Methods). This RNA was used for transcriptomic analysis of *M. jannaschii*, which showed that gene expression was significantly different between the three 80 °C treatments (10 mM iron-sulfide, MMC medium and sterile water, experiments 5a–c, Supplementary Table 1), indicating that each condition was associated with different physiological states (Fig. 3b). The sedimentary iron-sulfide chemical garden transcriptomes uncovered biological (analysis of similarity $P = 0.001$) and technical variation in between replicates exceeding that in controls (Fig. 3b), but nonetheless show a reproducible and unique gene expression profile induced by iron-sulfide chemical gardens. Key genes that were overexpressed by *M. jannaschii* in the chemical gardens reflect the H_2-dependent nature of *M. jannaschii* metabolism.

In contrast to the MMC medium, 120 genes were downregulated in *M. jannaschii* grown in sedimentary iron-sulfide chemical gardens, whereas 57 genes were downregulated in *M. jannaschii* cells grown in chemical gardens compared to the water controls (experiment 5, Fig. 4 and Supplementary Table 1). However, numerous genes encoding key enzymes of the H_2-dependent and CO_2-fixing acetyl-CoA pathway for methanogenesis were overexpressed in cells grown in chemical gardens when compared to the controls (Fig. 4 and Supplementary Tables 2 and 3). A total of 34 and 46 genes were overexpressed in cells grown in chemical gardens as compared to MMC medium (Fig. 4a and Supplementary Table 2) and water (Fig. 4b and Supplementary Table 3), respectively. The conditions of the chemical garden promoted the expression of the acetyl-CoA pathway in *M. jannaschii* compared to other cellular processes. There were 96 genes upregulated and 241 genes downregulated in *M. jannaschii* cells grown in MMC medium at the optimal 80 °C compared to MMC media at 25 °C (Extended Data Fig. 3).

The overexpressed genes of the methanogenic acetyl-CoA pathway (Fig. 4 and Supplementary Tables 2 and 3) consisted of CO dehydrogenase/CO-methylating acetyl-CoA synthase complex subunit beta (CODH/ACS), methyl-coenzyme M (methyl-COM) reductase subunits alpha/beta/gamma (*mcrA, mcrB* and *mcrG*), methyl-COM reductase operon proteins C/D (*mcrC* and *mcrD*), tetrahydromethanopterin *S*-methyltransferase subunits A–H (*mtr*A–H), formylmethanofuran dehydrogenase (*fmdA, fmdB* and *fmdC*), formylmethanofuran-tetrahydromethanopterin *N*-formyltransferase (*ftr*), acetyl-CoA decarbonylase/synthase complex subunits alpha/beta/gamma (ACDS) and coenzyme B–coenzyme M (CoB–CoM) heterodisulfide reductase subunits B/C (*hdrB* and *hdrC*). With the exception of only four genes (*mcrC*, *mcrD*, *ftr* and *hdrB,C*) all other acetyl-CoA pathway genes were overexpressed in the sedimentary iron-sulfide chemical gardens compared to both sterile water and MMC medium controls (Fig. 4). This shows that the chemical gardens were generally associated with a stimulated activity of the acetyl-CoA pathway in *M. jannaschii*, even compared to the growth conditions of the MMC medium, which was optimized for growth of hyperthermophilic methanogens[66] (Fig. 3a).

Methanogenesis requires several carbon carriers for the reduction of CO_2 to CH_4, which are the coenzymes methanofuran, tetrahydromethanopterin and CoM[18,71]. CoB is not a carbon carrier but is also required in the terminal step of methanogenesis[71]. Next to methane production through CO_2 fixation, the acetyl-CoA pathway also produces the metabolic intermediate acetyl-CoA, which is for example a precursor to lipids and pyruvate[72]. The key multi-enzyme complex involved in the acetyl-CoA formation is CODH/ACS[36,41] where CODH catalyses the CO_2 reduction to CO and ACS catalyses the C–C bond formation from CO and a methyl group to form acetyl-CoA[73]. This process allows methanogens to use CO as a carbon source. The multi-enzyme complex ACDS, which was also overexpressed in our sedimentary

https://doi.org/10.1038/s41559-025-02676-w

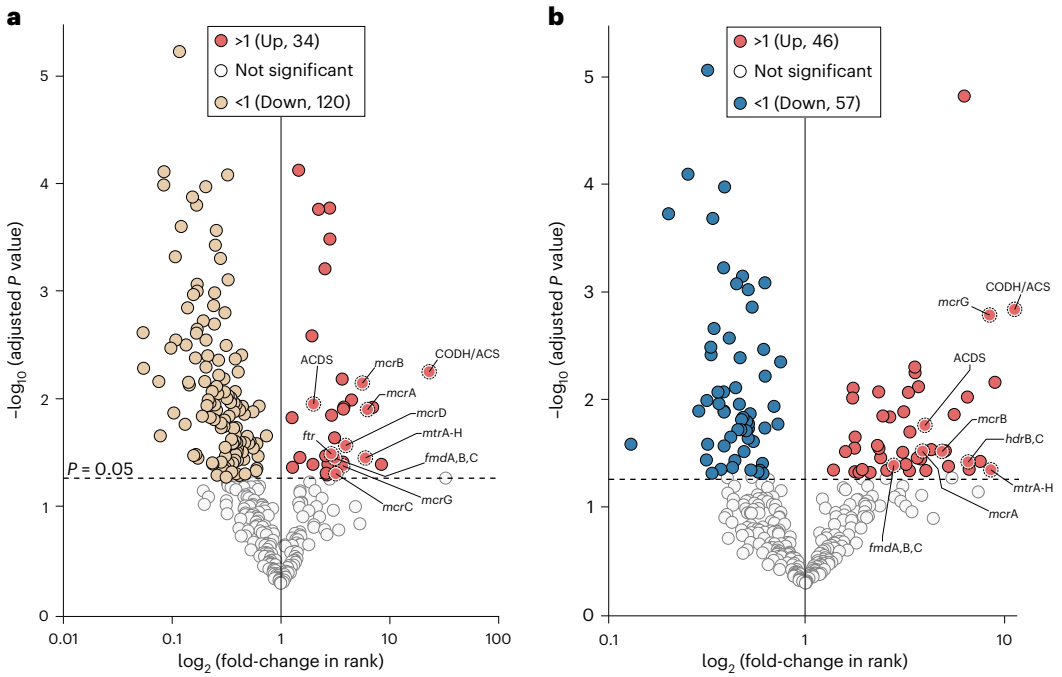

Fig. 4 | Volcano plot analysis of gene expression of *M. jannaschii* transcriptomes in the iron-sulfide chemical gardens. Gene expression is compared to two sets of controls (experiments 5a–c, Supplementary Table 1). **a**, Significant overexpression of genes ($n = 34$, $P < 0.05$) in *M. jannaschii* transcriptomes from 80 °C iron-sulfide chemical gardens (red, experiment 5a) relative to the MMC medium (beige, experiment 5c) ($P = 0.05$, one-sided *t*-test). **b**, Significant overexpression of genes ($n = 46$, $P < 0.05$) in *M. jannaschii* transcriptomes from 80 °C iron-sulfide chemical gardens (red, experiment 5a) relative to sterile water negative controls (blue, experiment 5b) ($P = 0.05$, one-sided *t*-test). The vertical line separates expressed genes that either increased or decreased in rank in the chemical gardens, the dotted horizontal line represents the *P* value cutoff for determining statistical significance. Overexpressed genes in the chemical gardens that are part of the methanogenic acetyl-CoA pathway are labelled. The full spellings of the gene acronyms of the acetyl-CoA pathway are provided in Supplementary Tables 1 and 2. Note that the genes of the methanogenic acetyl-CoA pathway were only overexpressed in the iron-sulfide chemical gardens, and were overexpressed relative to the MMC medium and sterile water negative controls.

iron-sulfide chemical gardens (Fig. 4), catalyses the reversible cleavage of acetyl-CoA in methanogens[74]. Electrons for the methanogenic acetyl-CoA pathway primarily come from H_2 (ref. 71). Considering that the genes responsible for the enzymatic conversions for most of these steps were overexpressed in the iron-sulfide chemical gardens, it appears that this chemolithoautotrophic pathway in *M. jannaschii* was probably driven by the abiotic H_2 released during the formation of mackinawite and greigite in the chemical gardens.

Interestingly, under the non-growing physiological state in sterile H_2O we observed an overexpression of some genes that encode enzymes of the acetyl-CoA pathway when compared to growth in MMC medium only (Extended Data Fig. 4 and Supplementary Table 4). This might indicate that non-growing archaeal cells experiencing H_2 limitation and/or nutrient limitation can maintain a physiological readiness to quickly react to suddenly appearing favourable growth conditions in a hydrothermal environment[66,75].

The key enzyme complex CODH/ACS (Fig. 4), which is necessary to make cell carbon[18], contains metal sulfur clusters affine with structure iron-sulfide minerals including greigite[36,64]. Although CODH/ACS was overexpressed when cultivated in sterile H_2O controls compared to MMC medium (Extended Data Fig. 4), the overexpression was six times higher in the chemical gardens (Fig. 4) by comparison. Specifically, CODH/ACS transcript levels had a fold-increase of 11.6 (one-sided *t*-test, $P = 0.0014$) in the iron-sulfide chemical garden relative to the sterile H_2O, compared to 1.9-fold increase (one-sided *t*-test, $P = 0.0007$) in sterile H_2O compared to MMC medium. This shows that while CODH/ACS is slightly overexpressed in a non-growing state, once the cells are placed into the iron-sulfide chemical garden, where they are alleviated from H_2 limitation, they increase the expression of CODH/ACS even more as well as other genes of the acetyl-CoA pathway. This further supports the conclusion that the cells remain physiologically ready for growth even if the cells are temporarily in a non-growing state.

Overexpression of *fmd*, *ftr* and *mtr*A–H in the iron-sulfide chemical gardens is notable considering that they are part of the first CO_2-reduction steps that take place in the acetyl-CoA pathway[71]. This is consistent with the stable isotope labelling experiment showing fixation of $^{13}CO_2$ by *M. jannaschii* in the iron-sulfide chemical gardens (Fig. 2c). Interestingly, *mtr*A–H, *fmd* and *ftr* were only overexpressed in cells cultivated in chemical gardens (Fig. 4), but not in the sterile water controls compared to MMC medium (Extended Data Fig. 4 and Supplementary Table 4), indicating an enhancement of the CO_2-reduction step by iron-sulfide conditions. This suggests that the iron-sulfide chemical garden promoted carbon fixation by *M. jannaschii*, which is consistent with the exponential growth observed in the iron-sulfide chemical gardens (Fig. 3a). No additional bicarbonate was added to the iron-sulfide chemical gardens and therefore some of the overexpression of *fmd*, *ftr* or *mtr*A–H relative to MMC medium could be a response to lower CO_2 levels and carbon limitation. However, this cannot explain the overexpression of genes in these cells compared to the sterile H_2O controls (because they also did not receive additional bicarbonate). Thus, it seems likely that the iron-sulfide chemical garden is a major factor influencing the overexpression of these genes.

Mcr catalyses the reduction of methyl-CoM with CoB to methane in the last step of the acetyl-CoA pathway, which is coupled to the formation of the heterodisulfide (CoM–S–S–CoB)[32,76,77]. Genes encoding all subunits of the mcr protein were overexpressed in the iron-sulfide chemical gardens relative to MMC medium and sterile H_2O controls (Fig. 4 and Supplementary Tables 2 and 3). In contrast, only the beta subunit was overexpressed in the sterile H_2O control compared

to MMC medium and its expression level was comparably lower (Supplementary Table 4). We also detected overexpression of two *mcr* operon proteins D and G in the iron-sulfide chemical garden relative to MMC medium.

The heterodisulfide reductase gene (*hdr*) was only overexpressed in an active growing state compared to a non-active growing state (iron-sulfide chemical garden relative to sterile H_2O, Fig. 4b). It was not overexpressed when comparing actively growing states to one another, specifically comparing the iron-sulfide chemical gardens to the MMC medium (Fig. 4a). This shows that hdr was important during active growth and not during dormancy. Hdr is an important iron-sulfur protein in the acetyl-CoA pathway that catalyses the reversible reduction of the heterodisulfide (CoM–S–S–CoB) back to CoM–SH and CoB–SH with H_2 leading to the formation of methane[76,78]. The overexpression of these acetyl-CoA pathway genes *mcr* and *hdr* is furthermore consistent with the stable isotope labelling of $^{13}CH_4$ which was produced by *M. jannaschii* in the iron-sulfide chemical gardens (Fig. 2c). *M. jannaschii* overexpressed a disproportionally higher percentage of genes assigned to archaeal clusters of orthologous genes (arCOGs)[79] involved in energy production and conversion and translation in iron-sulfide chemical gardens compared to the controls (Extended Data Fig. 5). All these results indicate that cellular control of the acetyl-CoA pathway responsible for energy conservation and CO_2 fixation was overexpressed in the chemical gardens (Fig. 4a). These experimental results support metabolic and evolutionary models based on phylogenomic reconstructions of LUCA, indicating that the acetyl-CoA pathway was present in LUCA, which might have lived in a hydrothermal environment[31,34].

Furthermore, it has been determined that reduced iron can promote electron transfer from H_2 to ferredoxin, which might have been important for cellular energy metabolism via the acetyl-CoA pathway before the emergence of enzymes and cofactors[80]. It therefore seems possible that reduced iron-sulfides could also facilitate electron transfer between H_2 and ferredoxin in *M. jannaschii*, which would help to explain how *M. jannaschii* can achieve exponential growth in the iron-sulfide chemical garden.

We compared the effect of temperature to iron-sulfide environments as a factor that might influence the overexpression of genes involved in the acetyl-CoA pathway. Gene expression of *M. jannaschii* at 80 and 25 °C (experiments 5c,d and Supplementary Table 1) in MMC medium was different (Fig. 3b). Temperature is known to have a strong effect on the gene expression of thermophilic archaea[75]. In our experiments, a total of 96 genes were overexpressed at 80 °C compared to 25 °C (experiment 5, Supplementary Table 1), with two of the overexpressed genes indirectly involved in regulation of the methanogenic acetyl-CoA pathway (Extended Data Fig. 3). These include methyl-COM reductase system component A2 (*atw*A), which is an ATP-binding protein[81], and an NADPH-dependent F420 reductase (*npd*G). Despite *M. jannaschii* being a hyperthermophile, the number of overexpressed acetyl-CoA pathway-associated genes at high temperature ($n = 2$) was lower compared to the iron-sulfide experiments ($n = 11$). This indicates that the iron-sulfide chemical garden environment had a larger positive influence on the activity of the H_2-dependent acetyl-CoA pathway metabolism relative to temperature.

While the genes encoding the acetyl-CoA pathway in the sedimentary iron-sulfide chemical garden were overexpressed relative to MMC medium, the growth rate of *M. jannaschii* was lower in the chemical gardens by comparison (Fig. 3a). The slower growth rate could be explained by the presence of additional bicarbonate (the carbon source), micronutrients, vitamins and trace metals supplied in the MMC medium, and excluded in the iron-sulfide chemical gardens (which only received $FeCl_2$ and Na_2S).

To conclude, the physiology of many methanogenic archaea is defined by H_2-dependent syntrophy, where H_2 is produced by a partner organism[82]. This relationship, whereby both partner organisms live together in a metabolic partnership, is considered to have an ancient origin[83]. Our results suggest, that on the early Eoarchaean Earth abiotic iron-sulfide geochemistry could have replaced H_2-producing syntrophic partner organisms and provide an abiotic H_2 source for H_2-dependent methanogenic archaea. This could have been an ancient precursor to modern syntrophic partnerships, whereby H_2 is sourced from biological fermentations.

Outlook

We provide experimental testing of a key aspect of hydrothermal and iron-sulfide-rich environments for the emergence of life, namely that abiotic H_2 produced in a sedimentary iron-sulfide chemical garden could have provided sufficient energy to fuel the survival and growth of Archaea in an Eoarchaean hydrothermal environment. Our results show that abiotic H_2 produced by iron-sulfide mineral redox reactions is sufficient to promote exponential chemolithoautotrophic growth of a hyperthermophilic methanogen under ferruginous conditions. This physiological response was explained by the overexpression of acetyl-CoA pathway-encoding genes by *M. jannaschii* in the sedimentary iron-sulfide chemical gardens and an exergonic CO_2-fixation pathway that has been described as a 'free lunch that you are paid to eat'[84]. Our findings provide experimental support for theories[36,85,86] predicting that the extreme and energy-limited conditions of iron-sulfide-rich environments of the Eoarchaean would have promoted an acetyl-CoA pathway-based metabolism. Our study points to FeS–Fe_3S_4 chemical gardens as potential hatcheries of life, primordial environments that could theoretically support a continuous evolution of the first metabolizing cells, through the progenote, to a methanogen.

Methods

The hyperthermophilic methanogen *M. jannaschii*[52] (DSM strain 2661, German Collection of Microorganisms and Cell Cultures GmbH) was cultivated in an MMC growth medium[68], which was prepared at the Institute of Microbiology and German Archaea Centre at the University of Regensburg (Supplementary Methods). The strain was recultivated from the Bacteria Bank Regensburg and adopted to the medium by at least two serial transfers in MMC. The stationary-phase cell cultures were used to inoculate the experiments that are part of this study.

In total, five different sets of experiments were executed (Supplementary Table 1). Throughout our paper we refer to these experiments as: experiment 1, chimney formation (Fig. 1a); experiment 2, abiotic H_2 formation (Fig. 2a and Extended Data Fig. 2); experiment 3, stable isotope labelling (Fig. 2b,c); experiment 4, *M. jannaschii* colonization and growth curve (Figs. 1b and 3a); and experiment 5, transcriptomics (Figs. 3b and 4 and Extended Data Figs. 3–5) and mineralogical analysis (Fig. 1c–f and Extended Data Fig. 1).

A detailed chimney formation protocol for experiment 1 is in Supplementary Methods. In experiment 2 and 3 (Supplementary Table 1), gas measurements of $^{13}CO_2$, $^{13}CH_4$ and H_2 were performed using a GC-MS QP2020 NX connected to a headspace autosampler (Shimadzu) (see Supplementary Methods for protocol).

In experiment 4 (Supplementary Table 1) we compared the growth of *M. jannaschii* in the sedimentary iron-sulfide chemical garden at 80 °C (experiment 4a) to its growth in MMC medium (experiment 4c) as a positive control. As an additional negative control, we also measured the growth of *M. jannaschii* in sterile water (experiment 4b). The sterile water negative control accounted for the dilution factor introduced in the chemical garden, making the presence of iron-sulfide the only difference between both experiments 4a and 4b. Using the chemical garden from experiment 4a we tested the colonization of *M. jannaschii* on the iron-sulfide particles (Fig. 1b). Cell counts and particle attachment were visualized using an inverted fluorescence microscope (Leica Thunder Imager DMi) based on autofluorescence of the coenzyme F420 present in *M. jannaschii*[87].

In experiment 5 (Supplementary Table 1) we compared the transcriptomic response of *M. jannaschii* at 80 °C in the sedimentary iron-sulfide chemical garden (experiment 5a) to the gene expression in MMC medium (experiment 5c) as a positive control and sterile water (experiment 5b) as a negative control. Furthermore, we performed transcriptomes on stationary-phase cultures stored at 25 °C (experiment 5d) as an additional low temperature comparison. Similar to experiment 4 the sterile water negative control was used to account for the dilution factor introduced by inoculating the stationary-phase culture into the chemical garden, making the presence of iron-sulfide the only difference between experiments 5a and 5b.

In experiment 5, RNA was extracted using the Direct-zol RNA Microprep kit (ZYMO Research)[75], with several changes to the protocol to improve RNA extraction from the chemical gardens. Phosphate was added to reduce adsorbtion of RNA to the iron-sulfide minerals and chloroform was added to improve RNA recovery (Supplementary Methods). Transcriptomes were prepared using the Revelo RNA-Seq kit (Tecan) and raw reads were mapped against the annotated genome of *M. jannaschii*[88] using BLASTx with DIAMOND[89] to measure gene expression levels.

The mineralogy of sedimentary iron-sulfide chemical gardens (experiment 5a, Supplementary Table 1) was analysed using Raman spectroscopy according to previously reported methods[47] and SEM with an EDX detector (protocol in Supplementary Methods). Full details on transcriptome preparations, bioinformatic analysis, cell counts, gas analysis, Raman spectroscopy, EDX analysis and MMC medium preparations are provided in Supplementary Methods[90,91].

Reporting summary

Further information on research design is available in the Nature Portfolio Reporting Summary linked to this article.

Data availability

Transcriptome data have been deposited in the NCBI short read archive under Bioproject ID PRJNA1157004.

Code availability

All code used in this study is available via GitHub at https://github.com/williamorsi/bioinformatics_code_orsi.

References

1. Lennie, A. R., Redfern, S. A., Schofield, P. F. & Vaughan, D. J. Synthesis and Rietveld crystal structure refinement of mackinawite, tetragonal FeS. *Mineral. Mag.* **59**, 677–683 (1995).
2. Hunger, S. & Benning, L. G. Greigite: a true intermediate on the polysulfide pathway to pyrite. *Geochem. Trans.* **8**, 1 (2007).
3. Lennie, A. R. et al. Transformation of mackinawite to greigite: an in situ X-ray powder diffraction and transmission electron microscope study. *Am. Mineral.* **82**, 302–309 (1997).
4. Drobner, E., Huber, H., Wächtershäuser, G., Rose, D. & Stetter, K. O. Pyrite formation linked with hydrogen evolution under anaerobic conditions. *Nature* **346**, 742–744 (1990).
5. Heinen, W. & Lauwers, A. M. Organic sulfur compounds resulting from the interaction of iron sulfide, hydrogen sulfide and carbon dioxide in an anaerobic aqueous environment. *Orig. Life Evol. Biosph.* **26**, 131–150 (1996).
6. Russell, M. J. & Hall, A. The emergence of life from iron monosulphide bubbles at a submarine hydrothermal redox and pH front. *J. Geol. Soc.* **154**, 377–402 (1997).
7. White, L. M., Bhartia, R., Stucky, G. D., Kanik, I. & Russell, M. J. Mackinawite and greigite in ancient alkaline hydrothermal chimneys: identifying potential key catalysts for emergent life. *Earth Planet. Sci. Lett.* **430**, 105–114 (2015).
8. Dodd, M. S. et al. Evidence for early life in Earth's oldest hydrothermal vent precipitates. *Nature* **543**, 60–64 (2017).
9. Papineau, D. et al. Metabolically diverse primordial microbial communities in Earth's oldest seafloor-hydrothermal jasper. *Sci. Adv.* **8**, eabm2296 (2022).
10. Russell, M. J., Hall, A. J. & Turner, D. In vitro growth of iron sulphide chimneys: possible culture chambers for origin-of-life experiments. *Terra Nova* **1**, 238–241 (1989).
11. Barge, L. M. et al. From chemical gardens to chemobrionics. *Chem. Rev.* **115**, 8652–8703 (2015).
12. Klein, F., Tarnas, J. D. & Bach, W. Abiotic sources of molecular hydrogen on Earth. *Elements* **16**, 19–24 (2020).
13. Truche, L., McCollom, T. M. & Martinez, I. Hydrogen and abiotic hydrocarbons: molecules that change the world. *Elements* **16**, 13–18 (2020).
14. Corliss, J. B. et al. Submarine thermal springs on the Galapagos Rift. *Science* **203**, 1073–1083 (1979).
15. Baross, J. A. & Hoffman, S. E. Submarine hydrothermal vents and associated gradient environments as sites for the origin and evolution of life. *Orig. Life Evol. Biosph.* **15**, 327–345 (1985).
16. Corliss, J., Baross, J. & Hoffman, S. An hypothesis concerning the relationship between submarine hot springs and the origin of life on Earth. *Oceanol. Acta* **80**, 59–69 (1981).
17. Goldford, J. E., Hartman, H., Marsland, R. III & Segrè, D. Environmental boundary conditions for the origin of life converge to an organo-sulfur metabolism. *Nat. Ecol. Evol.* **3**, 1715–1724 (2019).
18. Martin, W., Baross, J., Kelley, D. & Russell, M. J. Hydrothermal vents and the origin of life. *Nat. Rev. Microbiol.* **6**, 805–814 (2008).
19. Yamamoto, M., Nakamura, R. & Takai, K. Deep-sea hydrothermal fields as natural power plants. *ChemElectroChem* **5**, 2162–2166 (2018).
20. Karson, J. A., Kelley, D. S., Fornari, D. J., Perfit, M. R. & Shank, T. M. *Discovering the Deep: A Photographic Atlas of the Seafloor and Ocean Crust* (Cambridge Univ. Press, 2015).
21. Li, Y., Kitadai, N. & Nakamura, R. Chemical diversity of metal sulfide minerals and its implications for the origin of life. *Life* **8**, 46 (2018).
22. Dick, G. J. The microbiomes of deep-sea hydrothermal vents: distributed globally, shaped locally. *Nat. Rev. Microbiol.* **17**, 271–283 (2019).
23. Petersen, J. M. et al. Hydrogen is an energy source for hydrothermal vent symbioses. *Nature* **476**, 176–180 (2011).
24. Reveillaud, J. et al. Subseafloor microbial communities in hydrogen-rich vent fluids from hydrothermal systems along the Mid-Cayman Rise. *Environ. Microbiol.* **18**, 1970–1987 (2016).
25. Preiner, M. et al. A hydrogen-dependent geochemical analogue of primordial carbon and energy metabolism. *Nat. Ecol. Evol.* **4**, 534–542 (2020).
26. Russell, M. J., Hall, A. J. & Martin, W. Serpentinization as a source of energy at the origin of life. *Geobiology* **8**, 355–371 (2010).
27. Lane, N., Allen, J. F. & Martin, W. How did LUCA make a living? Chemiosmosis in the origin of life. *BioEssays* **32**, 271–280 (2010).
28. Woese, C. R. Bacterial evolution. *Microbiol. Rev.* **51**, 221–271 (1987).
29. Ueno, Y., Yamada, K., Yoshida, N., Maruyama, S. & Isozaki, Y. Evidence from fluid inclusions for microbial methanogenesis in the early Archaean era. *Nature* **440**, 516–519 (2006).
30. Ciccarelli, F. D. et al. Toward automatic reconstruction of a highly resolved tree of life. *Science* **311**, 1283–1287 (2006).
31. Weiss, M. C. et al. The physiology and habitat of the last universal common ancestor. *Nat. Microbiol.* **1**, 16116 (2016).
32. Borrel, G., Adam, P. S. & Gribaldo, S. Methanogenesis and the Wood–Ljungdahl pathway: an ancient, versatile, and fragile association. *Genome Biol. Evol.* **8**, 1706–1711 (2016).
33. Varma, S. J., Muchowska, K. B., Chatelain, P. & Moran, J. Native iron reduces CO_2 to intermediates and end-products of the acetyl-CoA pathway. *Nat. Ecol. Evol.* **2**, 1019–1024 (2018).

34. Moody, E. R. et al. The nature of the last universal common ancestor and its impact on the early Earth system. *Nat. Ecol. Evol.* **8**, 1654–1666 (2024).
35. Fuchs, G. Alternative pathways of carbon dioxide fixation: insights into the early evolution of life? *Annu. Rev. Microbiol.* **65**, 631–658 (2011).
36. Russell, M. J. & Martin, W. The rocky roots of the acetyl-CoA pathway. *Trends Biochem. Sci.* **29**, 358–363 (2004).
37. Martin, W. F. Older than genes: the acetyl CoA pathway and origins. *Front. Microbiol.* **11**, 817 (2020).
38. Sojo, V., Herschy, B., Whicher, A., Camprubi, E. & Lane, N. The origin of life in alkaline hydrothermal vents. *Astrobiology* **16**, 181–197 (2016).
39. Wagner, T., Ermler, U. & Shima, S. The methanogenic CO_2 reducing-and-fixing enzyme is bifunctional and contains 46 [4Fe-4S] clusters. *Science* **354**, 114–117 (2016).
40. Eck, R. V. & Dayhoff, M. O. Evolution of the structure of ferredoxin based on living relics of primitive amino acid sequences. *Science* **152**, 363–366 (1966).
41. Ragsdale, S. W. & Pierce, E. Acetogenesis and the Wood–Ljungdahl pathway of CO_2 fixation. *Biochim. Biophys Acta* **1784**, 1873–1898 (2008).
42. Poulton, S. W. & Canfield, D. E. Ferruginous conditions: a dominant feature of the ocean through Earth's history. *Elements* **7**, 107–112 (2011).
43. Song, H. et al. The onset of widespread marine red beds and the evolution of ferruginous oceans. *Nat. Commun.* **8**, 399 (2017).
44. Krissansen-Totton, J., Arney, G. N. & Catling, D. C. Constraining the climate and ocean pH of the early Earth with a geological carbon cycle model. *Proc. Natl Acad. Sci. USA* **115**, 4105–4110 (2018).
45. Hutchison, W., Finch, A. A. & Boyce, A. J. The sulfur isotope evolution of magmatic-hydrothermal fluids: insights into ore-forming processes. *Geochim. Cosmochim. Acta* **288**, 176–198 (2020).
46. Kawasumi, S. & Chiba, H. Redox state of seafloor hydrothermal fluids and its effect on sulfide mineralization. *Chem. Geol.* **451**, 25–37 (2017).
47. Helmbrecht, V., Weingart, M., Klein, F., Braun, D. & Orsi, W. D. White and green rust chimneys accumulate RNA in a ferruginous chemical garden. *Geobiology* **21**, 758–769 (2023).
48. Russell, M. J. Green rust: the simple organizing 'seed' of all life? *Life* **8**, 35 (2018).
49. Crowe, S. A. et al. Sulfate was a trace constituent of Archean seawater. *Science* **346**, 735–739 (2014).
50. Marty, B., Avice, G., Bekaert, D. V. & Broadley, M. W. Salinity of the Archaean oceans from analysis of fluid inclusions in quartz. *C. R. Geosci.* **350**, 154–163 (2018).
51. Knauth, L. P. in *Geobiology: Objectives, Concepts, Perspectives* (ed. Noffke, N.) 53–69 (Elsevier, 2005).
52. Jones, W., Leigh, J., Mayer, F., Woese, C. & Wolfe, R. *Methanococcus jannaschii* sp. nov., an extremely thermophilic methanogen from a submarine hydrothermal vent. *Arch. Microbiol.* **136**, 254–261 (1983).
53. Bult, C. J. et al. Complete genome sequence of the methanogenic archaeon, *Methanococcus jannaschii*. *Science* **273**, 1058–1073 (1996).
54. Ver Eecke, H. C. et al. Hydrogen-limited growth of hyperthermophilic methanogens at deep-sea hydrothermal vents. *Proc. Natl Acad. Sci. USA* **109**, 13674–13679 (2012).
55. Topçuoğlu, B. D., Meydan, C., Nguyen, T. B., Lang, S. Q. & Holden, J. F. Growth kinetics, carbon isotope fractionation, and gene expression in the hyperthermophile *Methanocaldococcus jannaschii* during hydrogen-limited growth and interspecies hydrogen transfer. *Appl. Environ. Microbiol.* **85**, e00180–19 (2019).
56. Skinner, B. J., Erd, R. C. & Grimaldi, F. S. Greigite, the thio-spinel of iron; a new mineral. *Am. Mineral.* **49**, 543–555 (1964).
57. Lafuente, B. et al. The power of databases: the RRUFF project. *Highlights Mineral. Crystallogr.* **1**, 25 (2015).
58. Genchev, G. & Erbe, A. Raman spectroscopy of mackinawite FeS in anodic iron sulfide corrosion products. *J. Electrochem. Soc.* **163**, C333–C338 (2016).
59. Mielke, R. E. et al. Iron-sulfide-bearing chimneys as potential catalytic energy traps at life's emergence. *Astrobiology* **11**, 933–950 (2011).
60. Roberts, A. P., Chang, L., Rowan, C. J., Horng, C. S. & Florindo, F. Magnetic properties of sedimentary greigite (Fe_3S_4): an update. *Rev. Geophys.* https://doi.org/10.1029/2010rg000336 (2011).
61. Dekkers, M. J., Passier, H. F. & Schoonen, M. A. Magnetic properties of hydrothermally synthesized greigite (Fe_3S_4)—II. High-and low-temperature characteristics. *Geophys. J. Int.* **141**, 809–819 (2000).
62. Russell, M. J. & Ponce, A. Six 'must-have' minerals for life's emergence: olivine, pyrrhotite, bridgmanite, serpentine, fougerite and mackinawite. *Life* **10**, 291 (2020).
63. McGlynn, S. E., Mulder, D. W., Shepard, E. M., Broderick, J. B. & Peters, J. W. Hydrogenase cluster biosynthesis: organometallic chemistry nature's way. *Dalton Trans.* https://doi.org/10.1039/B821432H (2009).
64. Nitschke, W., McGlynn, S. E., Milner-White, E. J. & Russell, M. J. On the antiquity of metalloenzymes and their substrates in bioenergetics. *Biochim. Biophys. Acta* **1827**, 871–881 (1827).
65. Finklea, S. L., Cathey, L. & Amma, E. Investigation of the bonding mechanism in pyrite using the Mössbauer effect and X-ray crystallography. *Acta Crystallogr. A* **32**, 529–537 (1976).
66. Wirth, R., Luckner, M. & Wanner, G. Validation of a hypothesis: colonization of black smokers by hyperthermophilic microorganisms. *Front. Microbiol.* **9**, 524 (2018).
67. Klingl, A. et al. Analysis of the surface proteins of *Acidithiobacillus ferrooxidans* strain SP5/1 and the new, pyrite-oxidizing *Acidithiobacillus* isolate HV2/2, and their possible involvement in pyrite oxidation. *Arch. Microbiol.* **193**, 867–882 (2011).
68. Gambelli, L. et al. An archaellum filament composed of two alternating subunits. *Nat. Commun.* **13**, 710 (2022).
69. Rickard, D. & Luther, G. W. Chemistry of iron sulfides. *Chem. Rev.* **107**, 514–562 (2007).
70. Thiel, J., Byrne, J. M., Kappler, A., Schink, B. & Pester, M. Pyrite formation from FeS and H_2S is mediated through microbial redox activity. *Proc. Natl Acad. Sci. USA* **116**, 6897–6902 (2019).
71. Brock, T. D., Madigan, M. T., Martinko, J. M. & Parker, J. *Brock Biology of Microorganisms* (Prentice-Hall, 2003).
72. Muchowska, K. B., Varma, S. J. & Moran, J. Nonenzymatic metabolic reactions and life's origins. *Chem. Rev.* **120**, 7708–7744 (2020).
73. Can, M., Armstrong, F. A. & Ragsdale, S. W. Structure, function, and mechanism of the nickel metalloenzymes, CO dehydrogenase, and acetyl-CoA synthase. *Chem. Rev.* **114**, 4149–4174 (2014).
74. Gu, W., Gencic, S., Cramer, S. P. & Grahame, D. A. The A-cluster in subunit β of the acetyl-CoA decarbonylase/synthase complex from *Methanosarcina thermophila*: Ni and Fe K-edge XANES and EXAFS analyses. *J. Am. Chem. Soc.* **125**, 15343–15351 (2003).
75. Grünberger, F. et al. Uncovering the temporal dynamics and regulatory networks of thermal stress response in a hyperthermophile using transcriptomics and proteomics. *mBio* **14**, e02174–23 (2023).
76. Hedderich, R., Hamann, N. & Bennati, M. Heterodisulfide reductase from methanogenic archaea: a new catalytic role for an iron-sulfur cluster. *Biol. Chem.* **386**, 961–970 (2005).
77. Ermler, U., Grabarse, W., Shima, S., Goubeaud, M. & Thauer, R. K. Crystal structure of methyl-coenzyme M reductase: the key enzyme of biological methane formation. *Science* **278**, 1457–1462 (1997).

78. Wagner, T., Koch, J., Ermler, U. & Shima, S. Methanogenic heterodisulfide reductase (HdrABC-MvhAGD) uses two noncubane [4Fe-4S] clusters for reduction. *Science* **357**, 699–703 (2017).
79. Makarova, K. S., Wolf, Y. I. & Koonin, E. V. Archaeal clusters of orthologous genes (arCOGs): an update and application for analysis of shared features between Thermococcales, Methanococcales, and Methanobacteriales. *Life* **5**, 818–840 (2015).
80. Brabender, M. et al. Ferredoxin reduction by hydrogen with iron functions as an evolutionary precursor of flavin-based electron bifurcation. *Proc. Natl Acad. Sci. USA* **121**, e2318969121 (2024).
81. Prakash, D., Wu, Y., Suh, S.-J. & Duin, E. C. Elucidating the process of activation of methyl-coenzyme M reductase. *J. Bacteriol.* **196**, 2491–2498 (2014).
82. Schink, B. Energetics of syntrophic cooperation in methanogenic degradation. *Microbiol. Mol. Biol. Rev.* **61**, 262–280 (1997).
83. Martin, W. & Müller, M. The hydrogen hypothesis for the first eukaryote. *Nature* **392**, 37–41 (1998).
84. Shock, E. L., McCollom, T. & Schulte, M. D. in *Thermophiles* (eds Wiegel, J. & Michael, A. W. W.) 79–96 (CRC, 1998).
85. Martin, W. & Russell, M. J. On the origins of cells: a hypothesis for the evolutionary transitions from abiotic geochemistry to chemoautotrophic prokaryotes, and from prokaryotes to nucleated cells. *Philos. Trans. R. Soc. Lond. B* **358**, 59–85 (2003).
86. Wächtershäuser, G. in *The Molecular Origins of Life* (ed. Brack, A.) 206–218 (Cambridge Univ. Press, 1998).
87. Muralidharan, V., Rinker, K., Hirsh, I., Bouwer, E. & Kelly, R. Hydrogen transfer between methanogens and fermentative heterotrophs in hyperthermophilic cocultures. *Biotechnol. Bioeng.* **56**, 268–278 (1997).
88. Graham, D. E., Kyrpides, N., Anderson, I. J., Overbeek, R. & Whitman, W. B. Genome of *Methanocaldococcus* (*Methanococcus*) *jannaschii*. *Methods Enzymol.* **330**, 40–123 (2001).
89. Buchfink, B., Xie, C. & Huson, D. H. Fast and sensitive protein alignment using DIAMOND. *Nat. Methods* **12**, 59–60 (2015).
90. Widdel, F. Theory and measurement of bacterial growth. *Di Dalam Grundpraktikum Mikrobiol* **4**, 1–11 (2007).
91. Orsi, W. D. et al. Carbon assimilating fungi from surface ocean to subseafloor revealed by coupled phylogenetic and stable isotope analysis. *ISME J.* **16**, 1245–1261 (2022).

Acknowledgements

This work was supported by the Deutsche Forschungsgemeinschaft project OR 417/8-1 granted to W.D.O. The work was also supported in part by the Transregio Collaborative Research Center (CRC 235, 'Emergence of Life') Project-ID 364653263—TRR 235 granted to W.D.O. We thank W. Martin for comments on the original version of the paper.

Author contributions

V.H., R.R., D.G. and W.D.O. designed the experiments. V.H. performed the experiments. W.D.O. and V.H. analysed data. All authors commented on the paper and contributed to the writing process.

Funding

Open access funding provided by Ludwig-Maximilians-Universität München.

Competing interests

The authors declare no competing interests.

Additional information

Extended data is available for this paper at https://doi.org/10.1038/s41559-025-02676-w.

Supplementary information The online version contains supplementary material available at https://doi.org/10.1038/s41559-025-02676-w.

Correspondence and requests for materials should be addressed to William D. Orsi.

Peer review information *Nature Ecology & Evolution* thanks Julie Huber, Helene Ver Eecke and the other, anonymous, reviewer(s) for their contribution to the peer review of this work.

https://doi.org/10.1038/s41559-025-02676-w

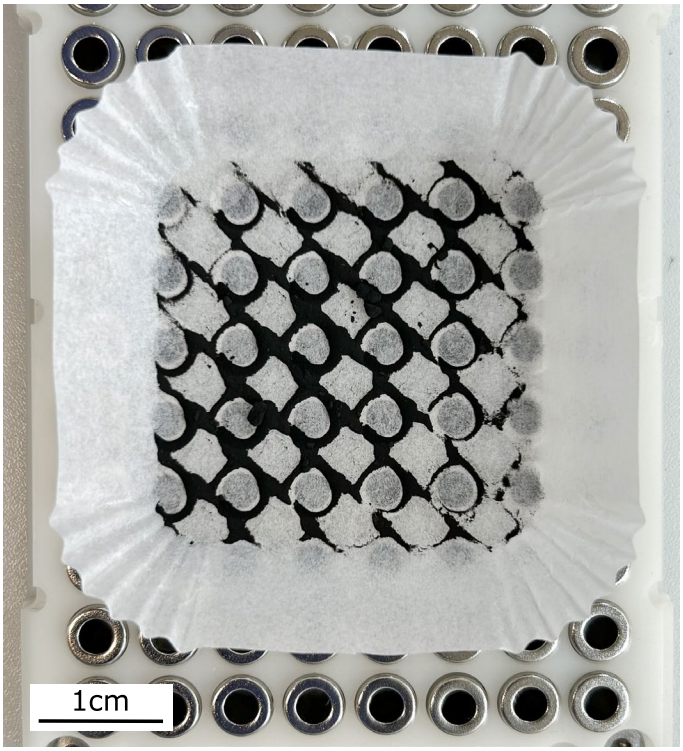

Extended Data Fig. 1 | Iron-sulfide particles are magnetic. Sedimentary iron-sulfide chemical garden precipitates align with magnetic rings on a ring magnet plate, showing the presence of the magnetic iron-sulfide mineral greigite (Fe_3S_4).

https://doi.org/10.1038/s41559-025-02676-w

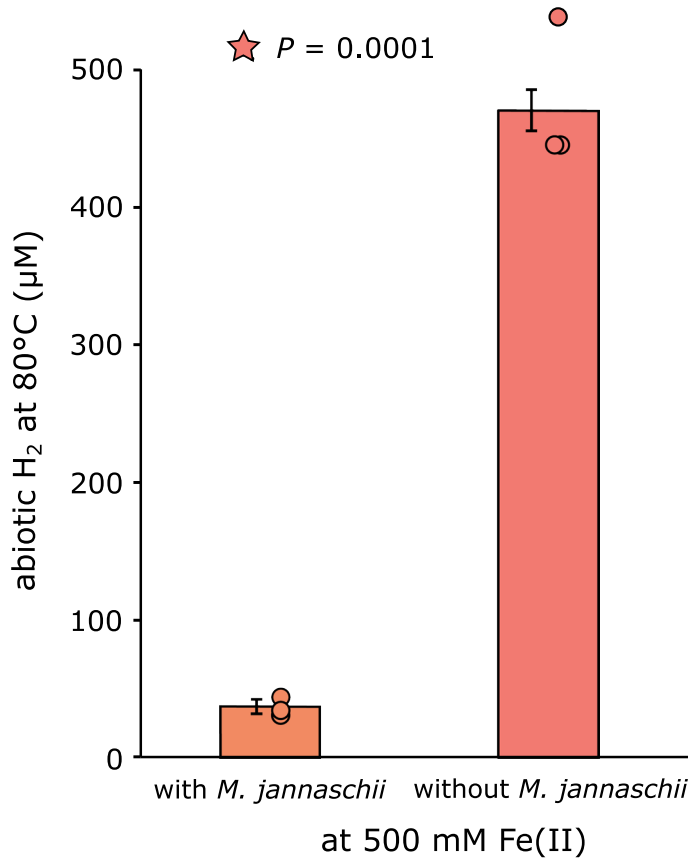

Extended Data Fig. 2 | Abiotic H_2 produced in the 500 mM sedimentary iron-sulfide chemical gardens at 80 °C with and without *M. jannaschii*. Error bars show standard error of the means across three biological replicates, P value is the result of a one-sided T-test.

https://doi.org/10.1038/s41559-025-02676-w

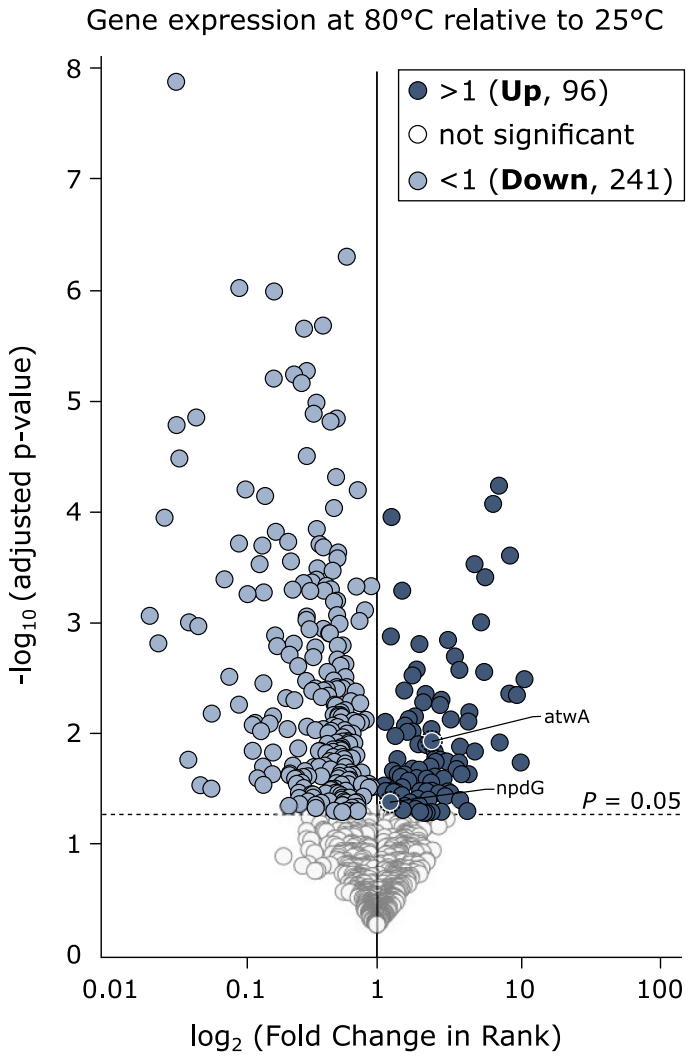

Extended Data Fig. 3 | Volcano plot analysis of gene expression of *M. jannaschii* transcriptomes in MMC Medium at 25 and 80 °C (*Experiments 5c, d*, Supplemental Table 1). Of all significant genes ($P = 0.05$, one-sided t-test), 96 are overexpressed at 80 °C (dark blue, *Experiment 5c*) compared to 25 °C. 241 genes were down regulated at 80 °C compared to 25 °C (light blue, *Experiment 5 d*). The vertical line separates expressed genes that either increased or decreased in rank in the MMC medium, the dotted horizontal line represents the *P*-value cutoff for determining statistical significance (one-sided T-test). Of all overexpressed genes, two are part of the methanogenic acetyl CoA pathway: methyl coenzyme M reductase system component A2 (*atw*A) and NADPH-dependent F420 reductase (*npd*G).

https://doi.org/10.1038/s41559-025-02676-w

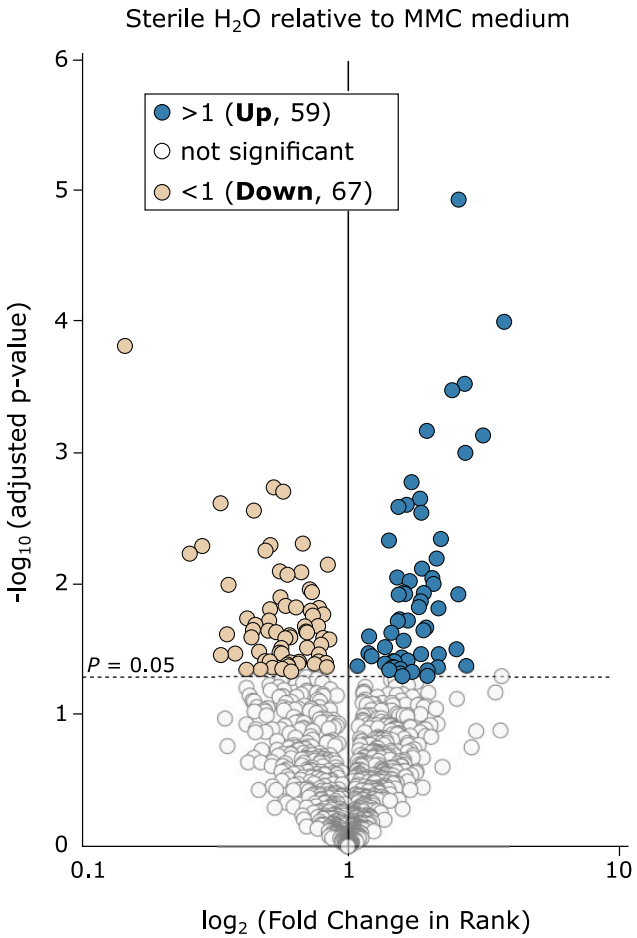

Extended Data Fig. 4 | Volcano plot analysis of gene expression of *M. jannaschii* transcriptomes in sterile water relative to MMC medium (*Experiments 5b, c*, Supplemental Table 1). Of all significant genes ($P = 0.05$, one-sided t-test), 59 are overexpressed in the sterile water controls (blue, *Experiment 5b*) compared to MMC medium (beige, *Experiment 5c*). Significantly overexpressed genes are listed in Supplemental Table 4. The full list of overexpressed genes is provided in Supplemental Table 4.

https://doi.org/10.1038/s41559-025-02676-w

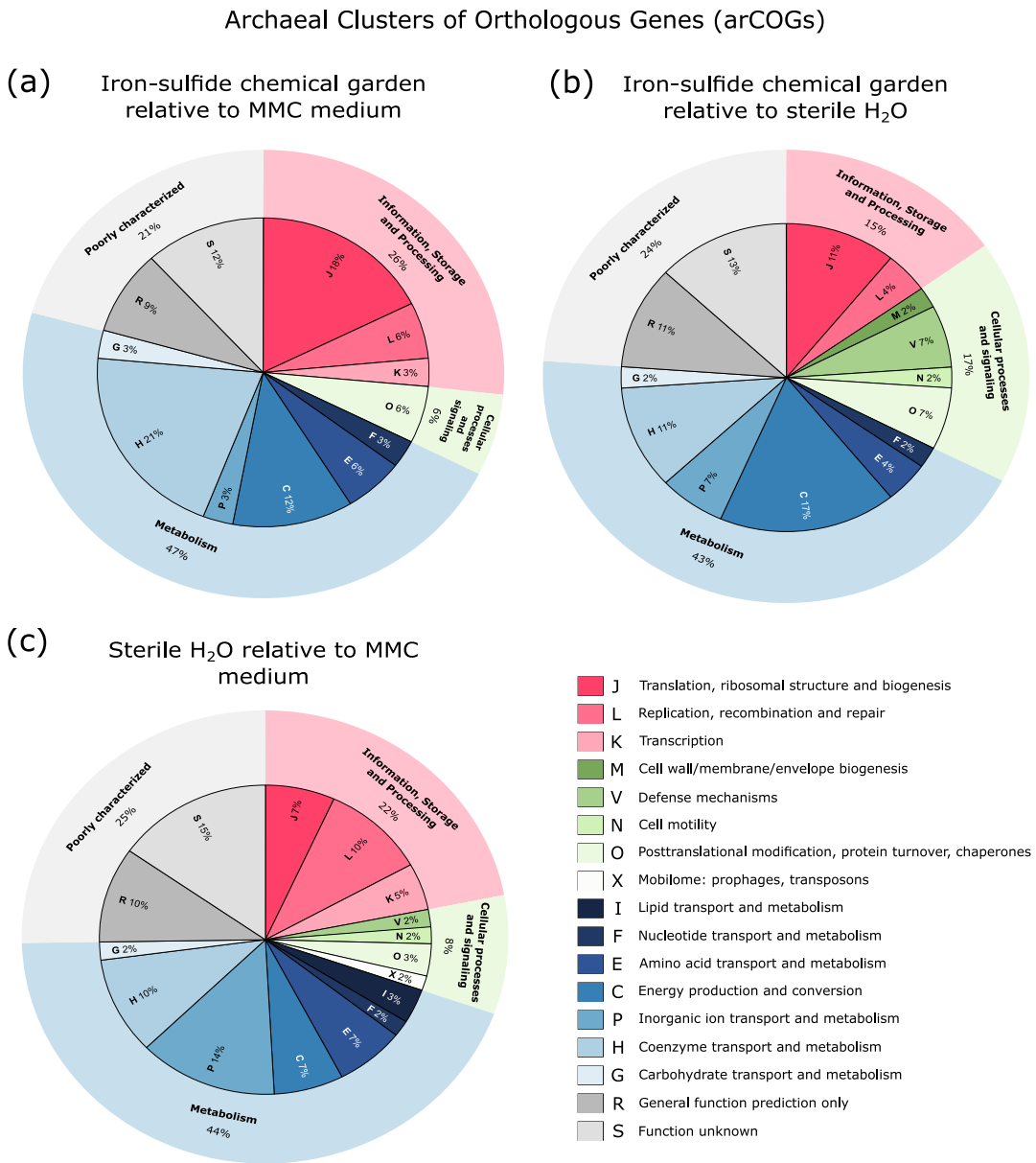

Extended Data Fig. 5 | Functional annotation of overexpressed genes. (*Experiments 5a-c*, Supplemental Table 1). For gene analysis, the arCOGs (Archaeal Clusters of Orthologous Genes) database was used[79]. (**a**) Out of 34 overexpressed genes in the sedimentary iron-sulfide chemical garden relative to MMC medium (Fig. 4a), the majority of genes has a function in metabolism (blue) or information, storage and processing (red), especially in coenzyme transport (H) and translation (J). (**b**) Out of 46 overexpressed genes in the sedimentary iron-sulfide chemical garden relative to sterile H_2O, most genes have a function in metabolism (blue), especially in energy production and conversion (C). Genes regulating cellular processes and signaling (green) make a proportion of 17 % of the overexpressed genes. (**c**) In the sterile H_2O controls relative to MMC medium, 59 genes were overexpressed, with 44 % having a metabolic function (blue).

nature portfolio

Corresponding author(s): William Orsi

Last updated by author(s): Nov 13, 2024

Reporting Summary

Nature Portfolio wishes to improve the reproducibility of the work that we publish. This form provides structure for consistency and transparency in reporting. For further information on Nature Portfolio policies, see our Editorial Policies and the Editorial Policy Checklist.

Statistics

For all statistical analyses, confirm that the following items are present in the figure legend, table legend, main text, or Methods section.

n/a	Confirmed	
☐	☒	The exact sample size (*n*) for each experimental group/condition, given as a discrete number and unit of measurement
☐	☒	A statement on whether measurements were taken from distinct samples or whether the same sample was measured repeatedly
☐	☒	The statistical test(s) used AND whether they are one- or two-sided *Only common tests should be described solely by name; describe more complex techniques in the Methods section.*
☒	☐	A description of all covariates tested
☒	☐	A description of any assumptions or corrections, such as tests of normality and adjustment for multiple comparisons
☐	☒	A full description of the statistical parameters including central tendency (e.g. means) or other basic estimates (e.g. regression coefficient) AND variation (e.g. standard deviation) or associated estimates of uncertainty (e.g. confidence intervals)
☐	☒	For null hypothesis testing, the test statistic (e.g. *F*, *t*, *r*) with confidence intervals, effect sizes, degrees of freedom and *P* value noted *Give P values as exact values whenever suitable.*
☒	☐	For Bayesian analysis, information on the choice of priors and Markov chain Monte Carlo settings
☒	☐	For hierarchical and complex designs, identification of the appropriate level for tests and full reporting of outcomes
☒	☐	Estimates of effect sizes (e.g. Cohen's *d*, Pearson's *r*), indicating how they were calculated

Our web collection on statistics for biologists contains articles on many of the points above.

Software and code

Policy information about availability of computer code

Data collection	Illumina software was used to demultiplex transcriptomes sequenced on the Illumina MiniSeq platform. CLC Genomics Workbench (version 9.5.4) was used to convert fastq files to fasta format, for the transcriptomes.
Data analysis	R was used to perform Principal Component Analysis and Analysis of Similarity (ANOSIM) statistical tests. DIAMOND was used to perform BLASTx searches of transcriptome reads (unassembled) against the M. jannaschii reference genome. A custom python script was used to summarize the BLASTx results per sample per gene in the reference genome and is available freely online through the LMU Open Science website (the URL is provided in the Methods of the paper). To analyze the RAMAN data and process the spectra, Labspec6 software was used. The cell counts were made using Las X software (part of the Leica inverted microscope) and ImageJ software. The stable isotope labeling data for gases was analyzed using the software pre-installed on the GCMS-QP2020 NX intrument.

For manuscripts utilizing custom algorithms or software that are central to the research but not yet described in published literature, software must be made available to editors and reviewers. We strongly encourage code deposition in a community repository (e.g. GitHub). See the Nature Portfolio guidelines for submitting code & software for further information.

Data

Policy information about availability of data

All manuscripts must include a data availability statement. This statement should provide the following information, where applicable:

- Accession codes, unique identifiers, or web links for publicly available datasets
- A description of any restrictions on data availability
- For clinical datasets or third party data, please ensure that the statement adheres to our policy

Transcriptome data have been deposited in the NCBI short read archive under Bioproject ID: PRJNA1157004

Research involving human participants, their data, or biological material

Policy information about studies with human participants or human data. See also policy information about sex, gender (identity/presentation), and sexual orientation and race, ethnicity and racism.

Reporting on sex and gender	Not applicable.
Reporting on race, ethnicity, or other socially relevant groupings	Not applicable.
Population characteristics	Not applicable.
Recruitment	Not applicable.
Ethics oversight	Not applicable.

Note that full information on the approval of the study protocol must also be provided in the manuscript.

Field-specific reporting

Please select the one below that is the best fit for your research. If you are not sure, read the appropriate sections before making your selection.

☐ Life sciences ☐ Behavioural & social sciences ☒ Ecological, evolutionary & environmental sciences

For a reference copy of the document with all sections, see nature.com/documents/nr-reporting-summary-flat.pdf

Ecological, evolutionary & environmental sciences study design

All studies must disclose on these points even when the disclosure is negative.

Study description	In total, five different sets of experiments were executed (see Supplemental Table 1). Throughout our manuscript we refer to these experiments as: Experiment 1 - chimney formation (Fig. 1a), Experiment 2 - abiotic H2 formation (Fig. 2a, Extended Data 3), Experiment 3 - stable isotope labeling (Fig. 2b, Extended Data 2), Experiment 4 - M. jannaschii colonization and growth curve (Fig. 1b and 3a) and Experiment 5 - transcriptomics (Fig. 3b, 4 and Extended Data 4) and mineralogical analysis (Fig. 1c-f).
Research sample	The hyperthermophilic methanogen Methanocaldococcus jannaschii was cultivated in a MMC growth medium, which was prepared at the Institute of Microbiology and German Archaea Centre at the University of Regensburg (see Supplemental Methods). The stationary phase cell cultures were used to inoculate the experiments that are part of this study.
Sampling strategy	A detailed chimney formation protocol for Experiment 1 is displayed in the SI Methods. In Experiment 2 and 3 (Supplemental Table 1) gas measurements of 13CO2, 13CH4, and H2 were performed using a GC-MS QP2020 NX connected to a headspace autosampler (Shimadzu) (see Supplemental Methods for protocol). In Experiment 4 (Supplemental Table 1) we compared the growth of M. jannaschii in the iron-sulfide chemical garden at 80 °C (Experiment 4a) to its growth in MMC medium (Experiment 4c) as a positive control. As an additional negative control, we also measured the growth of M. jannaschii in sterile water (Experiment 4b). The sterile water negative control accounted for the dilution factor introduced in the iron-sulfide chemical garden, making the presence of iron-sulfide the only difference between both Experiments 4a and 4b. Using the chemical garden from Experiment 4a we tested the colonization of M. jannaschii on the iron–sulfide particles (Fig. 1b). Cell counts and particle attachment were visualized using an inverted fluorescence microscope (Leica Thunder Imager DMi) based on autofluorescence of the coenzyme F420 present in M. jannaschii. In Experiment 5 (Supplemental Table 1) we compared the transcriptomic response of M. jannaschii at 80 °C in the iron-sulfide chemical garden (Experiment 5a) to the gene expression in MMC medium (Experiment 5c) as a positive control and sterile water (Experiment 5b) as a negative control. Furthermore, we performed transcriptomes on stationary phase cultures stored at 25 °C (Experiment 5d) as an additional low temperature comparison. Similar to Experiment 4 the sterile water negative control was used to account for the dilution factor introduced by inoculating the stationary phase culture into the iron-sulfide chemical garden, making the presence of iron-sulfide the only difference between Experiments 5a and 5b. In Experiment 5 RNA was extracted using the Direct-zol RNA Microprep kit (ZYMO Research), with several changes to the protocol to

improve RNA extraction from the iron-sulfide chemical gardens. Phosphate was added to reduce adsorbtion of RNA to the iron-sulfide minerals, and chloroform was added to improve RNA recovery (see Supplemental Methods). Transcriptomes were prepared using the Revelo RNA-Seq kit (Tecan) and raw reads were mapped against the annotated genome of M. jannaschii using BLASTx with DIAMOND to measure gene expression levels.
The mineralogy of iron-sulfide chemical gardens (Experiment 5a, Supplemental Table 1) was analyzed using Raman spectroscopy as described previously77 and scanning electron microscopy (SEM) with an EDX detector (protocol in SI Methods). Full details on transcriptome preparations, bioinformatic analysis, cell counts, gas analysis, Raman spectroscopy, EDX analysis and MMC medium preparations are provided in the Supplemental Methods.

Data collection	Data was collected either immediately after each experiment by Vanessa Helmbrecht, with the exception of transcriptome samples , EDX, and RAMAN analyses. EDX for elemental analysis was performed within 24 hours. For transcriptomes, the RNA was converted to cDNA libraries and sequenced within 2 to 3 weeks. For the RAMAN analyses, the measurements were made within 24 hours. The cell count data was collected within hourly intervals during growth experiment.
Timing and spatial scale	The cell count data was collected within hourly intervals during growth experiment that lasted 48 hours. The transcriptome data was collected after 4 hours of incubations. The RAMAN data from the minerals was collected after an 10 hour experiment. The stable isotope probing gas data was sampled every 2 hours over a 10 hour time interval. Chimney growth experiments lasted 1 hour.
Data exclusions	No data or samples were excluded.
Reproducibility	Biological replicates (n=3) were performed for all experiments.
Randomization	No randomization was performed, samples were grouped into biological replicates based on controlled conditions compared to a single factor that differed between the control and experiment.
Blinding	No blinding was performed.

Did the study involve field work? ☐ Yes ☒ No

Reporting for specific materials, systems and methods

We require information from authors about some types of materials, experimental systems and methods used in many studies. Here, indicate whether each material, system or method listed is relevant to your study. If you are not sure if a list item applies to your research, read the appropriate section before selecting a response.

Materials & experimental systems

n/a	Involved in the study
☒	☐ Antibodies
☒	☐ Eukaryotic cell lines
☒	☐ Palaeontology and archaeology
☒	☐ Animals and other organisms
☒	☐ Clinical data
☒	☐ Dual use research of concern
☒	☐ Plants

Methods

n/a	Involved in the study
☒	☐ ChIP-seq
☒	☐ Flow cytometry
☒	☐ MRI-based neuroimaging

Plants

Seed stocks	No plants were used.
Novel plant genotypes	No plants were used.
Authentication	No plants were used.